Investigation of Fundamental Mechanisms of Common-Mode Radiation from Printed Circuit Boards with Attached Cables

James L. Drewniak Todd H. Hubing Thomas P. Van Doren
Department of Electrical Engineering
University of Missouri–Rolla
Rolla, Missouri, 65401

Abstract

Fundamental mechanisms leading to common-mode radiation from printed circuit boards with attached cables have been studied. Two primary mechanisms have been identified, one associated with a differential-mode voltage that results in a common-mode current on an attached cable, and another associated with a differential-mode current that results in common-mode current on the cable. The two mechanisms are demonstrated through numerical and experimental results.

1 Introduction

Radiation from printed circuit boards with attached cables is of significant concern in meeting FCC regulations. Among the significant problems with common-mode radiation are common-mode currents induced on cables attached to printed circuit boards (PCB). The cable then acts as half of an antenna with the driving source located on the PCB or at the connector. The other half of the radiating structure is often difficult to determine but might include an extended portion of the ground, or other extended metal structures attached or effectively coupled to the PCB at RF frequencies. While the problem of common-mode radiation from cables attached to PCBs is well known, there is an incomplete knowledge of the fundamental mechanisms by which differential mode sources produce or induce common-mode currents on the cables. This makes diagnosing or anticipating and avoiding common-mode radiation problems from attached cables difficult. In addition, as computing speeds and powers continue to increase, the capability for modeling radiation with full-wave electromagnetic modeling codes at greater and greater detail exists. However, the possibility for modeling all features of a PCB design is in the distant future. A knowledge of coupling mechanisms is necessary to determine essential features that must be modeled to predict emissions reasonably well.

Paul has emphasized and demonstrated the need to consider and model common-mode currents in order to adequately predict radiation from printed circuit designs [1], [2]. Hubing et al. [3], as well as Hardin et al. [4] demonstrated the importance of circuit asymmetries in producing common-mode radiation. Dockey et al. [5], [6], and Drewniak et al. [7] have shown that voltage drops on ground conductors can result in common-mode radiation as a result of driving two portions of the extended ground against each other.

In this study, two coupling mechanisms that result in common-mode current on a cable attached to a PCB were studied. Examples of currents induced on wire extensions from a circuit using a numerical electromagnetics code are given for these two mechanisms. Simple wire circuits were constructed to demonstrate the mechanisms and to illustrate the dominance of one over the other in different cases. Finally, experimental results for an active circuit with a single processor are presented to illustrate the coupling source mechanisms.

2 Fundamental Mechanisms

Radiation requires an antenna coupled with a driving source. If either of these components is eliminated, or if the source is decoupled from the antenna, an ineffective radiator results. Minimizing common-mode radiation from printed circuit boards then becomes a problem of identifying potential common-mode driving sources and antennas, and rendering one or the other ineffective through a judicious choice of related design features. The common-mode radiators or "antennas" studied herein are of the dipole type, i.e., antennas with two distinct conductor halves at different RF potentials that are driven against each other to produce radiation.

Two fundmental source mechanisms for driving common-mode currents on cables attached to PCBs have been investigated. These source mechanisms have been denoted *voltage-* and *current*-driven mechanisms to distinguish the differential-mode quantity that provides the driving mechanism of the common-mode current on the attached cable. A wire circuit example that illustrates the physics of the current driven mechanism is shown in Figure 1 (a). An ideal voltage source is shown, so that the current is limited entirely by the inductance of the shorted loop. If the loop inductance is decomposed into partial inductances for the upper and lower conductors [8], [9] (assuming the vertical branches contribute negligibly small partial inductance), the large differential mode current through the partial inductance of the lower conductor results in a voltage drop. This voltage drop provides a voltage source that can drive common-mode current on the extended lower conductor as shown.

A wire circuit example illustrating the voltage driven

0-7803-1398-4/94/0000-0019 $4.00 © 1994 IEEE

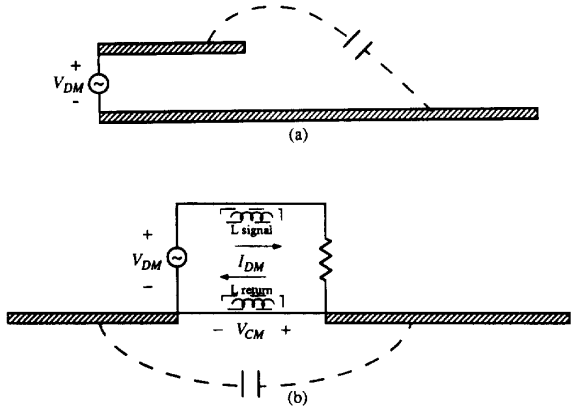

Figure 1: Wire circuit examples illustrating the physics of the a) current and b) voltage driven mechanisms.

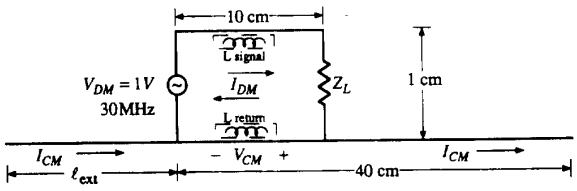

Figure 2: Representative wire circuit geometry investigated using NEC.

mechanism is shown in Figure 1 (b). In this case the differential-mode voltage provides the driving source that results in common-mode current. The extension of the return conductor beyond that of the signal conductor results in additional capacitance between the two conductors and an alternate current path. This alternate current path then results in common-mode current and common-mode radiation.

Numerical simulations on simple wire circuit configurations were conducted to test the physics described above. One circuit configuration is shown in Figure 2. The simulations were performed using the Numerical Electromagnetics Code (NEC) [10]. NEC is a proven full-wave electromagnetic modeling code based on the method of moments that has been found to be superior for wire geometries. While the circuits that were investigated were simple, they are representative of the wire-type antennas that typically arise with common-mode radiation problems in printed circuit designs. The source frequency was 30 MHz, and the source voltage was 1 V. In Figure 2 the geometry is short in terms of the free-space wavelength which is 10 m. The wire radius in the circuit is 0.8 mm. The common-mode current was computed simply by subtracting the current on the upper conductor from that on the lower conductor [9]. The common-mode current for an open circuit ($Z_L = \infty$) case of Figure 2 is shown in Figure 3 (a). The driving source for the common-mode antenna is V_{DM}, and the extent of the two halves of the conductor is sufficient to result in a significant common-mode current, with a peak current of approximately 75 μA. In this case

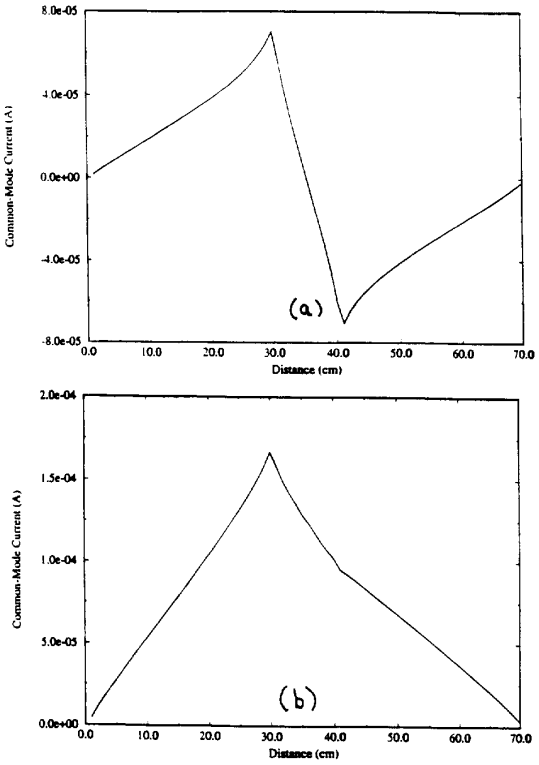

Figure 3: Common-mode current computed using NEC for a) open and b) short circuit cases of Figure 2. The origin is taken to be the left-most point on the lower conductor.

the common-mode current is a result of the differential-mode voltage source, i.e., the voltage-driven mechanism. As shown in Figure 3, the common-mode current is in opposite directions at opposite ends.

The common-mode current computed for the current driven mechanism with $Z_L = 0$ for the wire circuit geometry of Figure 2 is shown in Figure 3 (b). Again, the differential-mode current in the lower conductor branch of the differential-mode loop results in a voltage drop along this length. The voltage drop results in an equivalent common-mode voltage source that is distributed over the length of the conductor. This equivalent voltage source then drives the common-mode antenna, which is comprised of the two halves of the lower conductor.

3 Experimental Results

Test configurations to investigate the fundamental mechanisms of common-mode radiation described in the previous section were constructed and measurements conducted. An HP8753C network analyzer was employed for conducting experiments with passive wire circuit geometries. The experimental test layout is illustrated schematically in Figure 4. Port 1 of the network analyzer provided the source for the wire circuit, and the output of a common-mode current probe was input to Port 2. The source impedance for the device under test (DUT) was

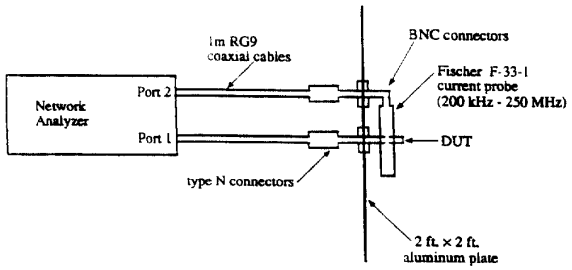

Figure 4: Experimental setup for investigation of circuit geometries with the HP8753C network analyzer.

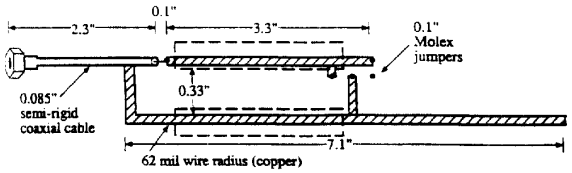

Figure 5: Wire circuit configuration for demonstrating the voltage and current driven mechanisms in printed circuit geometries.

the 50 Ω impedance of the network analyzer, as opposed to the ideal source used above in the numerical examples. A 2′ × 2′ square aluminum plate was used in all the measurement procedures in order to obtain a sufficiently large common-mode current to measure, and to provide a test environment from which repeatable measurements could be obtained. The measured common-mode current was not found to be a function of the network analyzer cable dressing when the aluminum plate was employed. The common-mode current was measured using a Fischer F-33-1 (200 $kHz - 250\ MHz$) current probe. The error correction capabilities of the HP8753C network analyzer enabled the transfer impedance of the current probe to be included in the calibration procedures.

The current and voltage driven mechanisms were investigated for a wire circuit. The geometry is shown in Figure 5. The Molex "jumper" connectors shown were employed to facilitate testing for open- and short-circuit loading conditions. While the geometry is still large relative to typical printed circuit dimensions, the circuit demonstrates the fundamental physics under investigation. The circuit source was provided by the network analyzer, and the common-mode current measured as previously described. The results for both open and short circuit loading conditions are shown in Figure 6 (a). The measured data in curves (1) and (2) are for open circuit loading conditions. Curve (1) is the result for the circuit with the 3.3″, 62 mil wire driven against the extended portion of the lower conductor (away from the ground plane), as well as against the semi-rigid coaxial cable and ground plane. The data of curve (2) was obtained with an added 1 *cm* wide, 7 *cm* long strip of aluminum tape on the upper conductor as indicated by the dashed rectangle in Figure 5. The increase in conductor area has increased the capacitance between the driven upper conductor and the semi-rigid coaxial cable (and ground).

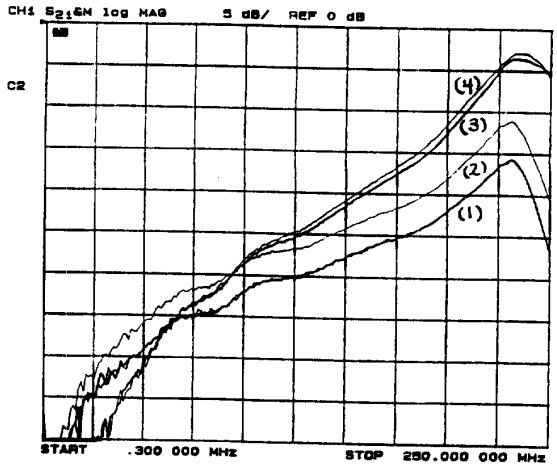

(a)

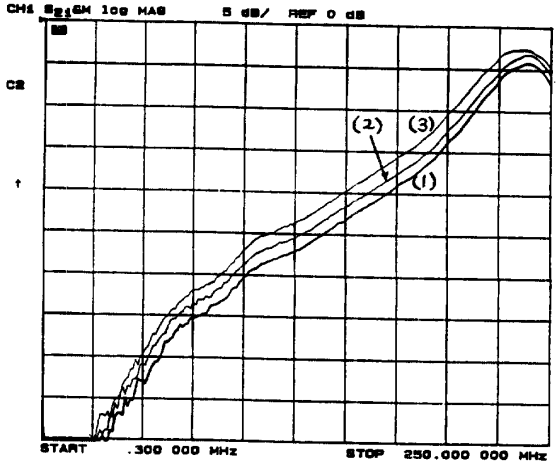

(b)

Figure 6: Results measured with the HP8753C network analyzer for the wire circuit geometry of Figure 5.

The measured data for short circuit loading conditions are shown in Figure 6 (a), curves (3) and (4), as well as Figure 6 (b). The current in the short circuited loop is limited by the 50 Ω source impedance, as well as the loop inductance, which results in an impedance of approximately $j50\ \Omega$ at 100 MHz. The measured results indicate for this geometry, that the current driven mechanism is dominant for frequencies above 100 MHz. The data in curve (3) of Figure 6 (a) is for the 62 mil conductor wire loop. Strips of aluminum tape 1 cm wide and 7 cm long were added to the top and bottom segments of the differential-mode current loop as shown by the dashed rectangles in Figure 5 with the resulting common-mode current shown in curve (4) of Figure 6. The driving source for the common-mode current on the extensions is the voltage drop produced by the differential-mode current through the partial inductance of the lower segment of the differential-mode loop.

The partial inductance of the lower or upper segments can be changed by adding a single aluminum tape strip to the segment as shown in Figure 5. The data for these cases are shown in Figure 6 (b). The data of curve (1) have the aluminum tape strip added to the bottom segment of the differential-mode loop, curve (2) is no strip added, and curve (3) is the strip added to the upper conductor. In cases (1) and (3) the differential-mode current is the same. The data illustrates what is expected for the current driven mechanism. When the aluminum strip is added to the upper conductor, more of the voltage dropped around the loop appears across the lower conductor as a result of lowering the partial inductance of the upper conductor. The voltage produced in the lower segment by the differential-mode current provides the driving source for the common-mode current on the antenna. Conversely, when the aluminum strip is added to the lower conductor, less of the total voltage is dropped along the lower segment. The driving source of the antenna is therefore reduced, and the resulting common-mode current is decreased, as observed from curve (1). Because of the distinct and different nature of these two mechanisms, changes in the circuit that decrease the CM current on the attached cable due to one mechanism, may increase the CM current due to the other mechanism.

The resonance observed in each curve is a result of a quarter-wavelength resonance corresponding to the length of the lower conductor above the ground plane, in both the open and short circuit cases. The wavelength at 235 MHz is approximately 128 cm, and a quarter wavelength is 32 cm. The length of the lower conductor above the ground plane is approximately 29 cm.

The common-mode driving source for the current-driven mechanism is the voltage drop incurred as a result of the differential-mode current inductance and hence the equivalent driving voltage for the cable can be reduced by widening the ground plane. This was investigated experimentally with a wire circuit geometry over a ground conductor as shown in Figure 7 (a). Measurements were obtained for a 1, 3, 5, 10, and 14 cm wide signal return conductor, and are shown in Figure 7 (b). The current is limited by the 50 Ω source impedance in series with the loop inductance. Using the approximate formula for a wire over an infinite ground plane, the loop impedance at 100 MHz was calculated to be approximately $j52\ \Omega$.

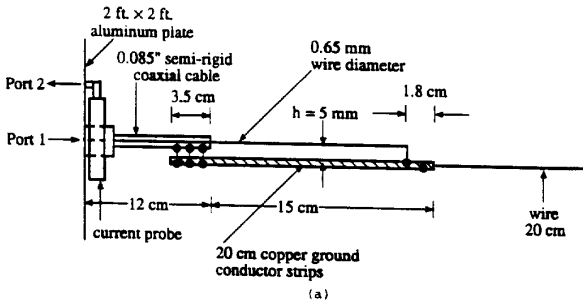

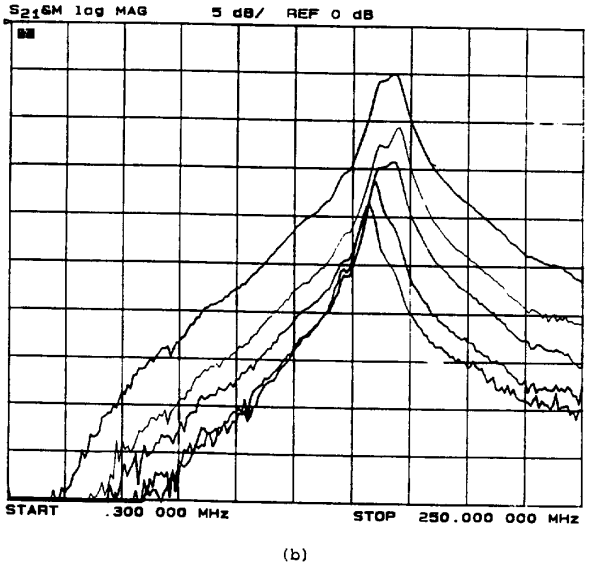

Figure 7: a) Circuit geometry for investigating the dependence of the current driven mechanism on the width of the signal return conductor. b) Data for signal return conductor widths of 1, 3, 5, 10, and 14 cm.

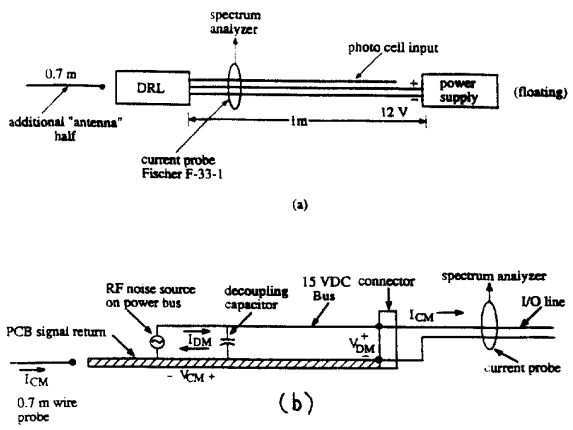

Figure 8: a) Experimental setup for common-mode current measurements on the leads to the DRL module. b) Reduced circuit model illustrating the fundamental mechanisms leading to common-mode radiation for the DRL module.

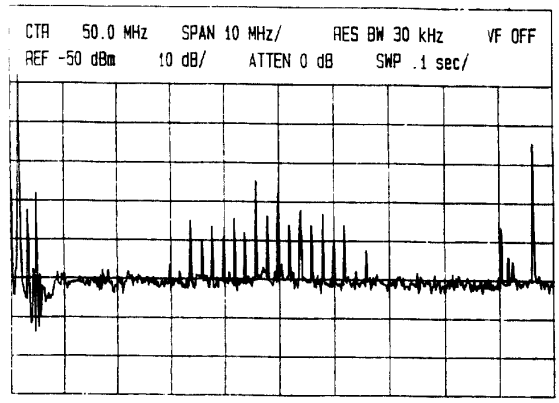

Figure 9: Common-mode current measured on the power and photocell input cable bundle.

It is observed that as the width of the signal return conductor is increased, the measured common-mode current decreases, which is consistent with a decreasing common-mode driving source.

The principles detailed in the above sections were applied to reduce the common-mode radiation from a production printed circuit design. The circuit, denoted the Daytime Running Lamp (DRL) module, produced significant common-mode radiation in a frequency band around 50 MHz. A schematic of the experimental setup is shown in Figure 8 (a). The DRL module was powered by a 12 V power supply. The power wires were 1 m long. A 1 m wire was also connected to the photocell input, and left unterminated to simulated the high impedance loading for daytime conditions. The common-mode current was measured 6″ from the DRL with the Fischer F-33-1 current probe connected to the spectrum analyzer, and is shown in Figure 9. Significant common-mode current on the cable bundle is observed in a band around 50 MHz. The signal shown in the data below 10 MHz and for $90-100$ MHz is measured when the DRL module is unpowered, and is not associated with common-mode radiation from the DRL module. A simple 0.085″ semi-rigid coaxial cable probe with the center conductor extended was employed for measuring the RF voltage on the 5 V side of the DC power bus. Measurements were taken at several points between the power pins of the single on-board IC module and the photocell input pin at the connector (which is connected to V_{CC}). Significant noise over the entire 100 MHz band was measured, with a slight peaking around 50 MHz. A 100 nF decoupling capacitor was placed at the connector across the photocell input and ground. The addition of the decoupling capacitor decreased the measured common-mode current by at least 25 dB. The dynamic range of the measurements is only 25 dB (initial common-mode current above the noise floor), and it is possible that the common-mode current is decreased even further. Both surface-mount and leaded 100 nF capacitors were employed, and found to produce the same results within the dynamic range of the measurements.

The dominant common-mode driving mechanism in this case is voltage driven. A simple model of the common-mode noise source and antenna on the DRL module is shown in Figure 8 (b). The driving source for the antenna is the differential-mode noise voltage on the 5 V power bus. This noise voltage, which is developed between the photocell input lead and ground as a result of the IC module switching (delta-I noise), is the differential-mode source that ultimately results in common-mode current on the photocell input and power lead cable bundle. The antenna is comprised of the photocell input lead and the extensive metal structures of several on-board relays that are directly connected to ground, as well as imbalances in the attached cable and the extended power ground.

The measured common-mode current on the described cable bundle for the off-the-shelf configuration of the DRL module was found to be dominated by the voltage driven mechanism. Upon further inspection of the reduced circuit model of Figure 8 (b), it is observed that the decoupling capacitor loop can provide a current driven mechanism type source, for driving a common-mode antenna. The large switching currents drawn by the IC module will produce a voltage drop on the ground conductor that can potentially drive two portions of the ground against one another (as two halves of an antenna). The common-mode voltage source that results from the differential-mode switching current is further increased in the attempt to eliminate the voltage driven mechanism by placing a decoupling capacitor between V_{CC} and ground at the connector. The length of the differential-mode loop is increased, as is possibly the differential mode-current by the addition of the 100 nF capacitor at the connector. An increase in the loop inductance is expected, and hence an increase in the voltage dropped along the return conductor. The noise voltage at four points along the ground conductor was measured with a 0.85″ semi-rigid coaxial cable probe, with a 100 nF decoupling capacitor connected between the photocell input and ground at the connector. A considerable difference in the magnitude of the RF noise voltage over the extent of the differential-mode switching current loop was observed. This variation in the voltage on the ground is consistent with what is expected with the

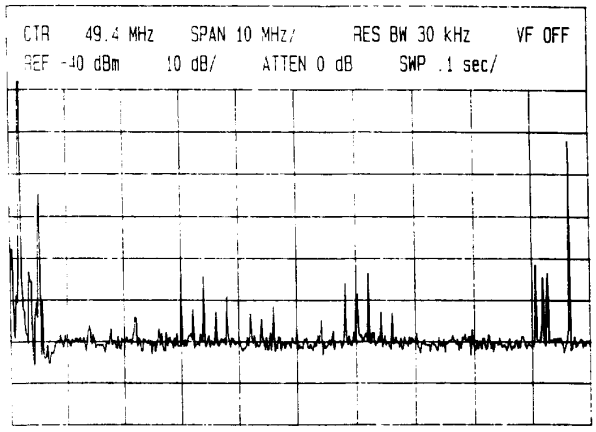

Figure 10: Common-mode current measured on the photocell input and power lead cable bundle with a 0.7 m wire attached to the ground conductor on the side of the IC package opposite the connector.

current-driven mechanism.

The decoupling capacitor loop, and the loop with the added 100 nF provides a common-mode voltage source that can drive an antenna. However, the judicious placement of the IC module in the far corner of the printed circuit board has effectively placed the common-mode voltage source very close to the end of the potential antenna. The high input impedance seen by the driving voltage source then results in unmeasurable common-mode current. A lower input impedance antenna can be artificially provided by connecting a wire to the ground conductor on the side of the IC package opposite the connector. This places the common-mode voltage source produced by the differential-mode current, approximately in the middle of the antenna, thereby lowering the input impedance. The common-mode current measured on the photocell input and power lead bundle for this configuration is shown in Figure 10. Common-mode current on the cable bundle is observed in frequency bands around 40 and 60 MHz.

4 Summary

Two mechanisms by which common-mode current can be induced on cables attached to PCBs have been demonstrated. These mechanisms are related to differential-mode voltages and currents on the the PCB or at the connector. It was shown numerically and experimentally that depending on the "antenna" which is being driven, and the signal levels, either mechanism can dominate. Because of the different nature of the current- and voltage-driven mechanisms, the approach to minimizing common-mode radiation problems depends on the dominant mechanism. Changes in the circuit that decreases CM radiation due to one mechanism, could in some cases, increase the CM current as a result of the other mechanism.

5 Acknowledgements

The authors greatfully acknowledge the support of General Motors in pursuing this research.

References

[1] C. R. Paul and D. R. Bush, "Radiated Emissions from Common-Mode Currents," *IEEE Electromagnetic Compatibility Symposium Digest*, September 1987.

[2] C. R. Paul, "A comparison of the contributions of common-mode and differential-mode currents in radiated emissions," *IEEE Trans. Electromagn. Compat.*, vol. 31, pp. 189-193, May 1989.

[3] T. H. Hubing and J. F. Kauffman, "Modeling the electromagnetic radiation from electrically small table-top products," *IEEE Trans. Electromagn. Compat.*, vol. 31, pp. 74-84, February 1989.

[4] K. B. Hardin, and C. R. Paul, "Decomposition of radiating structures using the ideal structure extraction method (ISEM)," *IEEE Trans. Electromagn. Compat.*, vol. 35, pp. 264-273, May 1993.

[5] R. W. Dockey, "Asymmetrical mode radiation from multilayer printed circuit boards," *EMC / ESD International Symposium Digest*, April 1992, pp. 247-251.

[6] R. W. Dockey and R. F. German, "New techniques for reducing printed circuit board common-mode radiation," *IEEE Electromagnetic Compatibility Symposium Digest*, August 1993, pp. 334-339.

[7] J. L. Drewniak, T. H. Hubing, and T. P. Van Doren, "Investigation of Fundamental Mechanisms Leading to Common-mode Radiation from Printed Circuit Boards," U. Missouri-Rolla EMC Lab Technical Rep. TR93-4-012R, May 1993.

[8] A. E. Ruehli, "Inductance calculations in a complex integrated circuit environment, " *IBM J. Research and Development*, vol. 16, pp. 470-481, 1972.

[9] C. R. Paul, *Introduction to Electromagnetic Compatibility*, Wiley-Interscience, New York, 1992.

[10] G. J. Burke and A. J. Poggio, *Numerical Electromagnetics Code (NEC) - Method of Moments*, Lawrence Livermore National Laboratory, January 1981.